Geophysical Research Letters

RESEARCH LETTER
10.1029/2019GL086059

Warm Temperature Extremes Across Greenland Connected to Clouds

Michael R. Gallagher[1,2], Hélène Chepfer[3], Matthew D. Shupe[1,2], and Rodrigo Guzman[4]

[1]Cooperative Institute for Research in Environmental Sciences, University of Colorado, Boulder, CO, USA, [2]Earth System Research Laboratory, NOAA, Boulder, CO, USA, [3]LMD/IPSL, Sorbonne Université, Ecole Polytechnique, CNRS, Paris, France, [4]LMD/IPSL, Ecole Polytechnique, CNRS, Sorbonne Université, Palaiseau, France

Key Points:
- Daily variability of opaque cloud cover and temperatures are closely linked
- Anomalies in opaque clouds and temperatures are tied to circulation regime
- The largest positive anomalies in both opaque clouds and temperatures relate to days with southerly transport

Correspondence to:
M. R. Gallagher,
michael.r.gallagher@noaa.gov

Citation:
Gallagher, M. R., Chepfer, H., Shupe, M. D., & Guzman, R.. (2020). Warm temperature extremes across Greenland connected to clouds. *Geophysical Research Letters*, *47*, e2019GL086059. https://doi.org/10.1029/2019GL086059

Received 31 OCT 2019
Accepted 20 FEB 2020
Accepted article online 24 FEB 2020

Abstract Greenland ice sheet melt is a large contributor to rising global sea level and melt is dependent on surface air temperature. Arctic temperatures are strongly coupled to clouds but spatial connections between clouds and temperature have yet to be established across Greenland. By mapping spaceborne lidar measurements and surface observations, it is shown that radiatively opaque clouds generally coincide with anomalously warm near-surface temperatures at Greenland sites. These results indicate that both temperatures over 0 °C as well as positive daily temperature anomalies relate to spatially extensive opaque cloud cover. While prior studies indicate that clouds enhance extreme melt events, this research shows that opaque cloud cover and surface warming are closely related across the Greenland ice sheet, particularly in the ablation region. These findings establish broadly the spatial relationships between opaque clouds and temperatures and demonstrate the importance of direct observations across Greenland.

Plain Language Summary Greenland ice sheet melt linked to temperatures is a large contributor to rising global sea level. Arctic temperatures are related to cloud cover but spatial changes in clouds and temperature for Greenland have yet to be quantified. Here we show that a specific type of clouds, determined by a measurement signature, coincide with warm temperatures at the Greenland surface. These results indicate that unusual occurrences of temperatures above 0 °C relate closely to cloud cover. While prior work has shown that clouds enhance extreme melt events, this research shows that cloud cover and surface warming are closely tied across the Greenland ice sheet, particularly in the regions of high mass loss. These findings establish the variability in clouds and demonstrate the importance of direct observations across Greenland.

1. Introduction

The Greenland ice sheet (GrIS) is losing approximately 181 gigatonnes of mass per year, contributing 1.32 mm to sea level rise annually, and is currently the fastest melting ice sheet in the cryosphere (Bamber et al., 2018; Shepherd et al., 2012). As Arctic warming continues, the GrIS is projected to add 5–10 cm to global sea level by the year 2100 (Fettweis et al., 2013). This increasing GrIS mass loss is primarily caused by surface melt, and atmospheric conditions are the main determinants of melt volume and extent (Andersen et al., 2015; Enderlin et al., 2014). More specifically, near-surface temperatures and radiation are the primary contributors to surface melt and thus the shrinking GrIS (Box et al., 2012).

Ground-based observations show that near-surface temperatures on the central GrIS are impacted by changes in cloud optical properties (Shupe & Intrieri, 2004). Although this influence is determined by a range of cloud properties (Miller et al., 2017), clouds with the largest effect on temperatures are typically opaque to longwave radiation, as has been observed across the Arctic (Sedlar et al., 2011; Shupe & Intrieri, 2004). As a result, radiatively opaque cloud cover enhances melt of the GrIS (Bennartz et al., 2013; Van Tricht et al., 2016). Despite the importance of radiatively opaque clouds, detailed cloud measurements are limited and opaque clouds have not been studied across the broader GrIS.

Due to the limited observations, regional models are typically used to quantify the spatial impact of opaque clouds on the GrIS (Franco et al., 2013; Solomon et al., 2017). However, model results for the GrIS are highly uncertain and satellite observations indicate that models poorly represent the variability of clouds in the Arctic and their surface impact (Cesana et al., 2012; Lacour et al., 2018; Lenaerts et al., 2017). Thus, present models alone are not sufficient to assess the spatial role of clouds in GrIS surface melt.

To address this pressing gap in our understanding, this study combines multiple targeted observational data sets with a unique set of analytical methods. Because previous research demonstrates that the daily variability of opaque clouds at Summit Station is linked to regional atmospheric circulation (Gallagher et al., 2018), the analysis presented here assesses regional circulation patterns for their impact on the spatial distribution of opaque cloud cover and the related variability of near-surface temperatures. This study is the first of its kind to observationally evaluate the impact of daily opaque cloud variability across the GrIS.

2. Methods and Data

The spatial variability in opaque clouds and their impact on the GrIS is the focus of this paper. Satellite observations of cloud opacity, near-surface temperature observations from automatic weather stations (AWS), and the daily variability of atmospheric circulation are combined together to connect these processes across the GrIS. Using self-organizing maps cloud observations are aggregated for days with similar atmospheric conditions, quantified here by regional sea level pressure (SLP) patterns. By aggregating satellite cloud measurements in this way, spatially complete maps of daily variability are constructed. Finally, near-surface temperature observations are also utilized to link this daily variability in cloud cover to the GrIS surface energy budget. Altogether, these observations and methodologies provide insight into the evolution of the atmosphere and its impact on clouds and temperatures of the GrIS.

Satellite cloud observations, provided by the CALIPSO (Cloud Aerosol Lidar and Infrared Pathfinder Satellite Observations) spaceborne lidar, are used here due to their extensive temporal and spatial coverage of Arctic clouds (Cesana et al., 2012; Chepfer et al., 2018; Kay et al., 2016; Kay & L'Ecuyer, 2013). Because this research is concerned with the impact of clouds on the GrIS surface, cloud opacity observations from CALIPSO from 2008 to 2016 are utilized here. First presented in Guzman et al. (2017) and Vaillant de Gúelis et al. (2017), these observations are part of the GCM-Oriented CALIPSO Cloud Product (CALIPSO-GOCCP; Chepfer et al., 2010; Cesana & Chepfer, 2013) and have been used in other similar polar cloud studies (Morrison et al., 2018). These data are optimal for use in this analysis because of a high correlation with the longwave cloud radiative effect (Guzman et al., 2017), making CALIPSO-GOCCP opaque cloud cover data a robust measure of cloud impacts on the GrIS.

In these data, radiatively opaque clouds are identified by the CALIPSO lidar surface echo caused from the reflection of the lidar beam at the surface. When no surface echo is detected, the measurement of the atmospheric profile is marked as opaque as the beam was scattered before reaching the Earth's surface. Thus, the cloud is opaque when the lidar signal is fully attenuated, which typically corresponds to a cloud LW emissivity of 0.8 to 0.9 (Vaillant de Gúelis et al., 2017). In this analysis, opaque cloud percentages are calculated across $1° \times 1°$ grid cells. The opaque cloud cover percentage is derived by comparing the number of profiles without a surface echo in a grid cell to the total number of profiles in that cell. This gridded opaque cloud cover percentage is used here to quantify the daily variability in optically thick clouds across the GrIS. A detailed description of the retrieval methodologies for opaque cloud cover data is available in Guzman et al. (2017).

AWS observe a multitude of parameters to constrain the surface energy budget, including broadband radiation and temperature. Due to the difficulty of obtaining accurate radiation measurements at unmanned sites in the harsh Arctic environment, this study focuses on the robust near-surface temperature observations from AWS overlapping the time period of CALIPSO measurements. A map of the stations used is included in Figure 1a. In this 2008–2016 time period two AWS networks were in operation on the GrIS. Nine AWS from the Greenland Climate Network were used in this analysis, for which site details and methodologies can be found in Steffen et al. (1996). Seven AWS from the Program for Monitoring the Greenland Ice Sheet maintained by the Geological Survey of Denmark and Greenland were also used, for which site details and methodologies can be found in Van As (2011). From these networks, only sites with greater than 75% coverage for the time period 2008–2016 were used for their sufficient temporal coverage. Temperature data were averaged daily for days with 80% or greater observational coverage.

To quantify regional atmospheric circulation, reanalysis data from the National Centers for Environmental Prediction and National Center for Atmospheric Research (Kalnay et al., 1996) were used. To categorize regional atmospheric circulation, gridded National Centers for Environmental Prediction and National Center for Atmospheric Research reanalysis daily SLP fields, beginning 1 January 1948 and ending 31

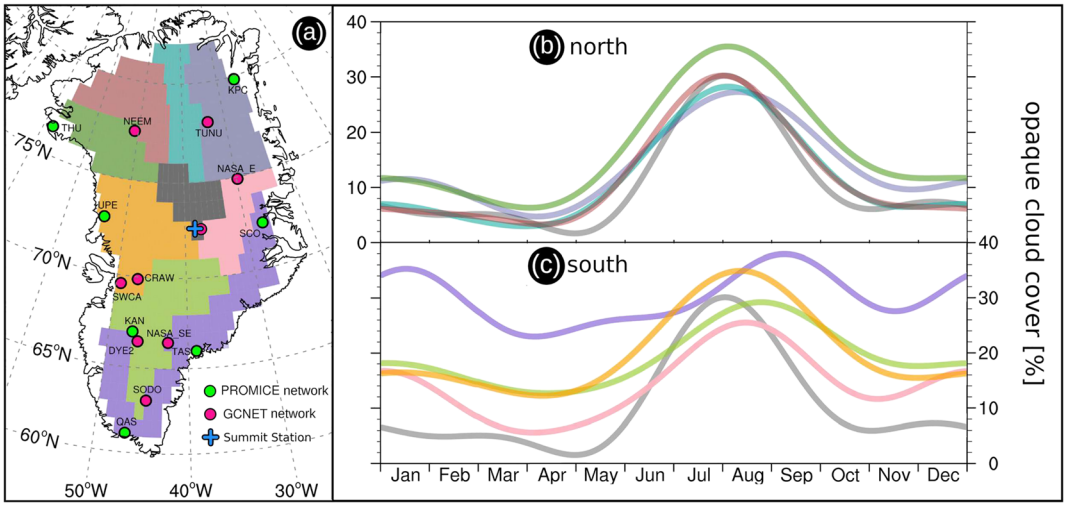

Figure 1. (a) Colored clusters indicate regions where observed daily opaque cloud cover is relatively homogeneous. Dots indicate surface site locations of temperature observations. (b and c) The annual cycle of opaque cloud cover derived using Fourier decomposition, for north and south cluster regions. The region near central Greenland, colored gray, is included on both plots to aid comparison.

December 2016, were used to construct a self-organizing map (SOM; Sheridan & Lee, 2011; Kohonen, 2013) following the methodology in Gallagher et al. (2018). This method, similar to work presented in Schuenemann and Cassano (2009) and Mioduszewski et al. (2016), allows for the grouping and analysis of processes by the regional atmospheric circulation state.

Due to the interannual variability of atmospheric circulation states, daily anomalies of cloud and temperature observations must be calculated with respect to the annual cycle. As a result of the brief observational record, this cannot be accomplished by constructing a traditional mean daily climatology. Instead, Fourier decomposition was used to identify time series components having variability on time scales greater than two weeks to produce annual cycles of observations. Anomalies were calculated by subtracting daily observations from this derived annual cycle, leaving variability that can be attributed to high-frequency changes in atmospheric circulation (Gallagher et al., 2018). Anomalies in this study refer to the difference between an observation and its expected annual background state, calculated using this method. For near-surface temperature observations at AWSs, an annual cycle can be derived using Fourier decomposition and available continuous time series temperature data.

Because satellite observations are made in narrow swaths across the GrIS on any given day, a more detailed approach is necessary to produce continuous time series of opaque cloud observations. In order to derive the necessary annual cycles, observations must be aggregated across regions where cloud cover can be identified as similar. Here nine unique regions of cloud variability across Greenland were identified using a machine learning clustering algorithm. To calculate opaque cloud anomalies, CALIPSO observations are aggregated for these regions, with the chosen number of nine balancing the identification of spatial features in opaque cloud cover with adequate spatial and temporal coverage of observations for each region. Simpler divisions into geographic regions such as “east” and “central” were tested and insufficiently captured the spatial variability of opaque clouds across the GrIS. Thus, this analysis would not be possible without this regional clustering methodology.

To identify these regions with machine learning algorithms, the covariance matrix of each $1° \times 1°$ pixel was calculated and this matrix was weighted by the mean seasonal values for the associated pixel. A clustering algorithm was then applied to the weighted covariance matrices for the identification of regional clusters of pixels with similar variability. Effectively, this is the upscaling and grouping of $1° \times 1°$ CALIPSO pixels, a methodology comparable to that described in Crane and Hewitson (2003). Spectral, self-organizing maps, k-means, and DBSCAN, clustering algorithms were tested, with spectral clustering chosen here due to its low internal cluster variance for identified regions. The regions, shown in Figure 1a, were identified using

the spectral clustering code available from the open source and freely available scikit-learn machine learning library (Pedregosa et al., 2011).

3. Results

3.1. Opaque Cloud Variability

Figure 1 presents the identified regions of similar opaque cloud variability and the opaque cloud annual cycles for each region. Anomalies for opaque cloud observations are calculated with respect to these annual cycles. The annual cycle of opaque clouds for the four regions north of 75° latitude is similar to that of the region over central Greenland surrounding Summit Station. Opaque cloud cover in these northern regions is maximum in late summer, with typically less than 10% occurrence of opaque clouds in winter. Regions south of 75° latitude differ from this significantly, with more opaque cloud cover during winter than for northerly regions. The most southerly coastal region has a distinct annual cycle, with approximately 30% opaque cloud cover year-round and maxima in both late January and early September.

Each of the regions in Figure 1a represents an area where sparse satellite observations can be aggregated to provide sufficient statistics for identifying characteristic annual cycles and thus calculate daily opaque cloud cover anomalies for the region. A particular CALIPSO opaque cloud observation is considered anomalously high or low according to its difference from that day in the annual cycle for the region of the observation. All uses of the word anomaly refer to values calculated relative to the annual cycles shown for opaque cloud cover in Figure 1.

This anomalous variability in observations of opaque cloud cover is attributed to regional circulation patterns identified by the SOM algorithm. The SOM classification of the common regional circulation patterns is presented in Figure 2a, and the associated anomalous opaque cloud cover attributed to each circulation pattern in the SOM is presented in Figure 2b. In Figure 2a the monthly distribution of pattern occurrences from 2008 to 2016 is given at the bottom of each panel, showing the important seasonal variability of each regional circulation state. Attributing opaque cloud cover anomalies to circulation state reveals a strong relationship between atmospheric circulation and the daily spatial variability of opaque cloud cover across the GrIS. The daily variability of opaque cloud cover is closely aligned with the location and strength of onshore atmospheric flow, where anomalies in opaque cloud cover are linked to the position and strength of cyclone centers around Greenland.

Three broad transport modes are identified within the SOM matrix. Circulation patterns surrounding pattern [a,3] represent cyclones to the east of the subcontinent with large SLP gradients, causing strong northerly meridional transport across the GrIS. These are known as “Icelandic Low” cyclones, a prominent feature of North Atlantic atmospheric circulation (Berdahl et al., 2018). Circulation patterns centered around [c,1] depict cyclones to the west of Greenland, causing strong southerly transport across the GrIS. Zonal transport patterns are centered around [d,4], with cyclones to the south of the subcontinent. In particular, the patterns causing more northerly transport over the GrIS occur most often in winter, while the southerly patterns are most frequent in summer. The patterns causing zonal transport over the GrIS occur in all seasons.

Strong connections are observed between southerly and northerly meridional transport and large anomalies in the corresponding spatial opaque cloud cover. For daily occurrences of southerly circulation patterns [c,1] and [d,1], large positive opaque cloud cover anomalies occur across southern and western Greenland, extending into the central GrIS, with negative anomalies on the north coast. Conversely, daily occurrences of strong northerly circulation patterns [a,3] and [a,4] relate to positive opaque cloud cover anomalies in the north and east with significant negative anomalies over the southern GrIS.

While meridional flow relates to large and consistent opaque cloud cover anomalies, zonal patterns surrounding circulation pattern [d,4] have a less clear relationship to opaque cloud cover. Zonal flow patterns, with low-pressure systems to the south of the subcontinent, relate to a relatively neutral opaque cloud cover state and thus minimize opaque cloud anomalies for occurrences of these patterns. Average opaque cloud anomalies for zonal patterns rarely exceed positive or negative 10% anywhere on the GrIS and have less spatial coherence.

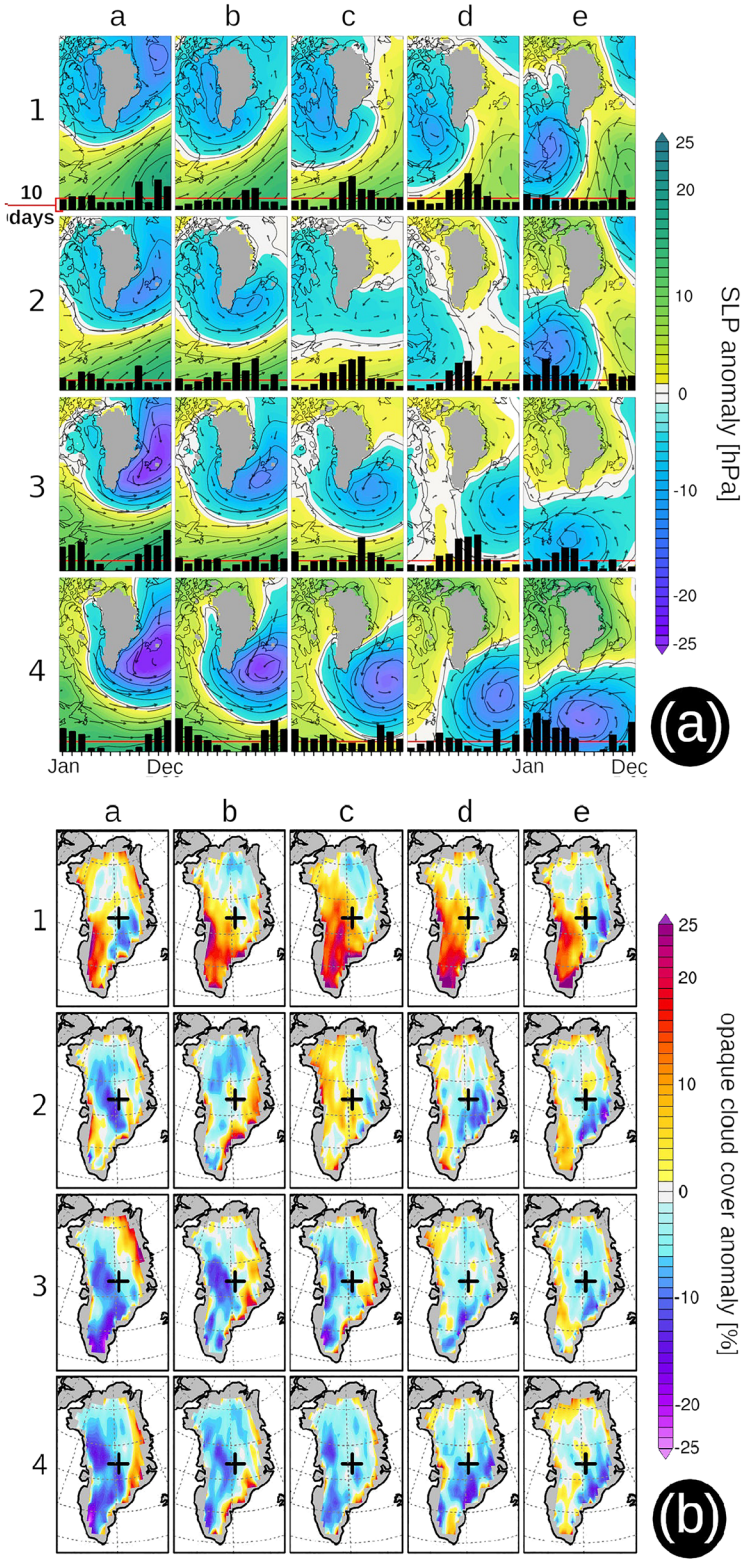

Figure 2. (a) Prevalent regional circulation patterns identified in sea level pressure reanalysis data, along with corresponding streamlines (arrows). Histograms on the bottom of each pattern in black indicate the total daily occurrences of each month throughout the year for the period of overlapping observations from 2008 to 2016. (b) Average observed daily opaque cloud cover anomaly from 2008 to 2016 at every 1° × 1° pixel for each circulation pattern in (a). Daily anomaly is defined relative to the annual cycle for each cluster shown in Figure 1. The cross gives the location of the in situ site at Summit Station to provide a geographical reference for comparison between plots.

More broadly, the results presented here highlight how regional atmospheric circulation interfaces with the topography of the GrIS. In regions of steep topography, onshore flow is shown to enhance cloud cover on the windward side of the orography and these enhanced opaque clouds are most prominent for circulation patterns causing southerly moisture transport. This is most clear when comparing positive opaque cloud anomalies occurring in western and eastern Greenland. On the eastern side of the GrIS, where the topography is steepest, opaque cloud anomalies are largest very near to the steep coastline. In contrast, on the gentler slope of the western side of the GrIS, positive opaque cloud anomalies extend significantly further inland, often crossing the majority of the GrIS. Finally, on the leeward side of the subcontinent, cloud cover is frequently anomalously negative for many of the circulation patterns with the larger negative anomalies likely tied to clearing under downslope flow.

These maps are a unique new result, demonstrating that the average daily spatial variability in opaque clouds caused by atmospheric circulation can be derived from sparse lidar satellite tracks. Because these results show that spatial opaque cloud cover variability is tied closely to atmospheric circulation, and prior detailed in situ studies indicate that opaque cloud cover impacts temperatures via radiative effects (Gallagher et al., 2018), the remainder of this paper examines spatial observations of temperature and their relationship to opaque clouds. Specifically, by mapping near-surface temperatures from AWS, we aim to show that daily synoptic atmospheric state, opaque cloud cover, and temperature variability are closely tied across the GrIS.

3.2. Clouds and Temperatures

Previous research has connected variability in opaque cloud cover on the central GrIS to near-surface temperature variability (Miller et al., 2017). Here observations of daily near-surface temperatures across the GrIS demonstrate that both extreme temperatures above 0 °C and large warm anomalies in general relate to circulation patterns with extensive opaque cloud cover anomalies (Figure 3a). Southerly atmospheric circulation patterns surrounding [c,1] lead to both extensive positive opaque cloud cover anomalies and positive temperature anomalies across the south and west GrIS, with daily temperature anomalies averaging 3 °C for pattern [c,1].

Temperature results in Figure 3a show that southerly circulation, as in [c,1] and [d,1], corresponds to large anomalies in both opaque cloud cover and temperatures. Consequently, annual occurrence distributions indicate that southerly patterns are most frequent during peak melt months of June, July, and August. Thus, circulation patterns leading to the largest positive temperature and opaque cloud cover anomalies occur when the GrIS is the most responsive to increased melt.

This enhanced effect occurs with considerable spatial variability. Coastal regions of the GrIS in the south and west are the primary zones of surface mass loss (van den Broeke et al., 2009). Circulation patterns surrounding [c,1] relate to large anomalies across this coastal ablation region, with an average opaque cloud cover anomaly of approximately 20%. Correspondingly, southerly circulation patterns also relate to the largest positive temperature anomalies across AWS sites in this coastal ablation region. In juxtaposition, for these southerly circulation patterns, negative opaque cloud anomalies in northern and northeastern Greenland relate to positive temperature anomalies for [c,1] and [c,2], and negative temperature anomalies for [e,1]. This spatial variability is inherently tied to interactions between atmospheric circulation, moisture transport, and the topography of the GrIS. In this way, Figures 2 and 3 provide a complete picture of the spatial relationship between clouds, temperatures, and the daily variability of atmospheric circulation.

Compared to southerly atmospheric circulation patterns, zonal transport patterns around [d,4] relate less clearly to the daily variability of opaque clouds and temperatures. Pattern [d,3], a zonal transport pattern occurring primarily in summer, averages minor decreases in spatial opaque cloud cover. Although opaque cloud cover anomalies are negative, a large number of [d,3] occurrences relate to temperatures above 0 °C, suggesting a circulation regime where clouds are not the primary contributor to warming. Conversely, the predominantly winter zonal pattern [e,4] relates to increased anomalous temperatures but with few occurrences of temperatures above 0 °C at observation sites. These subtle characteristics of zonal atmospheric circulation and resulting cloud and temperature impacts align closely with the results from prior in situ studies at Summit Station (Gallagher et al., 2018).

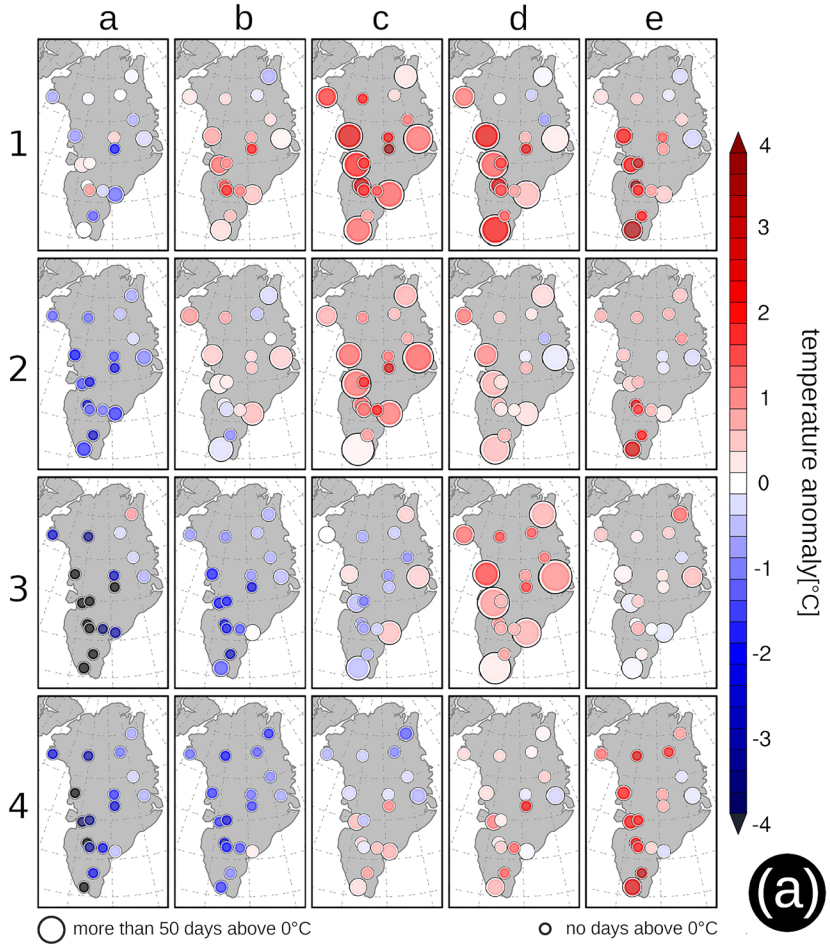

	a	b	c	d	e
1	0	2	8	2	2
2	0	3	2	1	0
3	0	0	0	1	0
4	0	0	0	0	0

(b)

Figure 3. (a) Average daily near-surface temperature anomaly from 2008 to 2016 for each circulation pattern. Daily anomaly is defined relative to the annual temperature cycle for each individual station. The size of the station dot corresponds to the number of days the station was above 0 °C during the occurrences of each pattern. (b) The total number of days where 50% or more of GrIS surface stations in (a) averaged above 0 °C, indicating which circulation patterns are related to broad and extreme warming.

Because this framework forms a complete description of the regional circulation, decreases in opaque cloud cover and temperatures can also be studied. Northerly transport circulation patterns surrounding [a,4] relate to large negative anomalies in opaque cloud cover and temperatures over much of the GrIS. For these northerly patterns, the spatial homogeneity and magnitude of opaque cloud cover and temperature anomalies is dependent on the strength and location of the cyclone east of the GrIS, with patterns showing positive opaque cloud cover anomalies at the coast near onshore atmospheric flow. Because of the generally cold temperatures in the north, these northerly patterns do not contribute significantly to melt. However, occurrences of circulation patterns causing anomalously cold temperatures over much of the GrIS can serve to inhibit melt by decreasing the subsurface temperatures (Miller et al., 2017).

Motivated by the spatial and temporal relationships between opaque cloud cover and temperatures revealed here, days with spatially extensive temperature extremes were investigated. Days where 8 or more of the 16 surface stations were above 0 °C are categorized to signify broad extreme warming events, similar to the recent extreme melt event seen in July 2012 (Nghiem et al., 2012). A total of 21 days from 2008 to 2016 reached this 50% threshold and these days are attributed to their corresponding atmospheric circulation (Figure 3b). The results show that for 16 of these 21 events, atmospheric circulation over the GrIS was in a southerly state with increased opaque cloud cover, represented by circulation patterns [b,1], [c,1], [d,1], and [e,1]. Zonal circulation pattern [d,3] related to only one such event. The 21 extreme days identified indicate that southerly transport frequently relates to broad opaque cloud cover as well as temperatures above 0 °C. While previous studies have shown that southerly transport favors melt over the GrIS (Mattingly et al., 2018; Oltmanns et al., 2019), these results show the detailed spatial correspondence between extreme warming events and cloud opacity for the first time.

4. Discussion and Conclusions

While these results provide novel insight into the spatial relationships between opaque clouds and near-surface temperatures, detailed spatial observations of clouds and their impact on the surface energy budget are not readily available to further investigate the processes that link cloud and surface conditions. Southerly transport brings enhanced opaque cloud cover over much of the GrIS, but also warm air advection and the transport of water vapor. Near-surface temperatures are impacted by all of these factors, as temperature advection, humidity, and cloud cover together alter the Arctic surface energy budget (Cox et al., 2015; Miller et al., 2017). The research presented here cannot analyze these process-based factors spatially across the GrIS using currently available observations. However, previous Arctic cloud studies at Summit Station in central Greenland (Miller et al., 2017), the Arctic Ocean (Sedlar et al., 2011; Shupe & Intrieri, 2004), and at other Arctic field sites (Shupe et al., 2015; Stone, 1997) have shown how opaque cloud cover over bright surfaces increases surface radiation and therefore near-surface temperatures. Additionally, specific case studies have shown a strong link between moisture advection, cloud formation, radiation, and GrIS melt (Bennartz et al., 2013; Neff et al., 2014). These detailed studies provide a foundation for understanding Arctic cloud impacts, and thus, results from this paper should be regarded in the context of these previous process-oriented studies relating opaque clouds to their surface impacts.

By studying cloud observations through the lens of regional SLP patterns, conclusions about clouds and temperature are made in the broader context of atmospheric circulation. Although opaque cloud cover is not observed for years outside 2008–2016, it is reasonable to assume that the relative spatial relationships described here between daily atmospheric circulation, opaque clouds, and temperatures remain true in the recent past and the near future. However, in decades to come, cloud cover and its impact may change due to the Arctic amplification of global warming and the future warmer, wetter Arctic (Serreze & Barry, 2011). On longer temporal scales, trends in atmospheric circulation and changes to the circulation patterns themselves have the possibility to modify conclusions presented here (Young et al., 2012).

Although the limited available in situ observations indicate that clouds contribute to increased energy transmission to the GrIS surface, some recent model studies have produced conflicting results (Riihelä et al., 2019). Van Tricht et al. (2016) used satellite observations of radiation integrated into the regional climate model RACMO2.3 to demonstrate that cloud impacts possibly reduce meltwater refreezing, and thus increase surface runoff. Conversely, Hofer et al. (2017) used trends in passive satellite observations of clouds

along with MAR to show that an observed trend in the reduction of clouds relates to a model trend in increased shortwave absorption for ablation regions of the GrIS, thus increasing melt production.

These dissonant conclusions highlight the challenge in modeling the spatially heterogeneous GrIS melt and the difficulty in validating model results with sparse observations. The research presented in this paper describes the correspondence between the daily variability of spatial opaque cloud cover and near-surface temperatures using high-quality, spatial cloud observations, but adequate observations to further describe the detailed processes do not exist. As a research community, further steps should be taken to understand and align these potentially conflicting results. To accomplish this, the most effective approach is to begin detailed long-term cloud studies in the ablation region of the GrIS. Results here highlight the unique spatial variability of opaque cloud cover across the GrIS, showing the ablation region to be a unique location to investigate processes impacted by opaque cloud cover.

Ultimately, to understand the long-term fate of the GrIS and its impact on sea level change, models must be improved to include accurate representation of clouds and their radiative effects. Alignment of regional Arctic models such as MAR with sophisticated observations is critical for supporting the improvement of global models and their predictive power. Data sets like these presented here are essential building blocks, providing the insight needed to improve and validate these models. This analysis highlights the spatial variability of GrIS cloud processes, demonstrates the importance of diverse and robust observations, and provides a proof-of-concept foundation for future analyses of sparse satellite observations over the GrIS and other similar domains.

Acknowledgments

This research was supported by National Science Foundation grants PLR-1303879, OPP-1801477, and PLR-1314156, and the NOAA Earth System Research Laboratory. Thanks to the Laboratoire de Météorologie Dynamique for their support and funding of international collaboration for this work. Thanks kindly to Jen Kay for her support and feedback. The GOCCP v3 products used here are available online through the GOCCP website (https://climserv.ipsl.polytechnique.fr/cfmip-obs/Calipso_goccp.html). Thanks to the teams who deploy and monitor the PROMICE and GCNET AWS networks. Sincere thanks to the reviewers of this paper for their thoughtful and thorough critiques. Data from the Programme for Monitoring of the Greenland Ice Sheet (PROMICE) and the Greenland Analogue Project (GAP) were provided by the Geological Survey of Denmark and Greenland (GEUS) at http://www.promice.dk. The GC-Net data were obtained from the Steffen Research Group and the Cooperative Institute for Research in Environmental Sciences at http://cires1.colorado.edu/science/groups/steffen/gcnet/order/admin/station.php. NCEP/NCAR reanalysis data were obtained from the NOAA/ESRL Physical Science Division in Boulder, Colorado, USA (http://www.esrl.noaa.gov/psd/).

References

Andersen, M. L., Stenseng, L., Skourup, H., Colgan, W., Khan, S. A., Kristensen, S. S., et al. (2015). Basin-scale partitioning of Greenland ice sheet mass balance components (2007–2011). *Earth and Planetary Science Letters*, *409*, 89–95. https://doi.org/10.1016/j.epsl.2014.10.015

Bamber, J. L., Westaway, R. M., Marzeion, B., & Wouters, B. (2018). The land ice contribution to sea level during the satellite era. *Environmental Research Letters*, *13*(6). https://doi.org/10.1088/1748-9326/aac2f0

Bennartz, R., Shupe, M. D., Turner, D. D., Walden, V. P., Steffen, K., Cox, C. J., et al. (2013). July 2012 Greenland melt extent enhanced by low-level liquid clouds. *Nature*, *496*(7443), 83–86. https://doi.org/10.1038/nature12002

Berdahl, M., Rennermalm, A., Hammann, A., Mioduszweski, J., Hameed, S., Tedesco, M., et al. (2018). Southeast Greenland winter precipitation strongly linked to the Icelandic low position. *Journal of Climate*, *31*(11), 4483–4500. https://doi.org/10.1175/JCLI-D-17-0622.1

Box, J. E., Fettweis, X., Stroeve, J. C., Tedesco, M., Hall, D. K., & Steffen, K. (2012). Greenland ice sheet albedo feedback: Thermodynamics and atmospheric drivers. *The Cryosphere*, *6*(4), 821–839. https://doi.org/10.5194/tc-6-821-2012

Cesana, G., & Chepfer, H. (2013). Evaluation of the cloud thermodynamic phase in a climate model using CALIPSO-GOCCP. *Journal of Geophysical Research: Atmospheres*, *118*, 7922–7937. https://doi.org/10.1002/jgrd.50376

Cesana, G., Kay, J. E., Chepfer, H., English, J. M., & de Boer, G. (2012). Ubiquitous low-level liquid-containing Arctic clouds: New observations and climate model constraints from CALIPSO-GOCCP. *Geophysical Research Letters*, *39*, L20804. https://doi.org/10.1029/2012GL053385

Chepfer, H., Bony, S., Winker, D., Cesana, G., Dufresne, J. L., Minnis, P., et al. (2010). The GCM-Oriented CALIPSO Cloud Product (CALIPSO-GOCCP). *Journal of Geophysics*, *115*, D00H16. https://doi.org/10.1029/2009JD012251

Chepfer, H., Noel, V., Chiriaco, M., Wielicki, B., Winker, D., Loeb, N., & Wood, R. (2018). The potential of a multidecade spaceborne lidar record to constrain cloud feedback. *Journal of Geophysical Research: Atmospheres*, *123*, 5433–5454. https://doi.org/10.1002/2017JD027742

Cox, C. J., Walden, V. P., Rowe, P. M., & Shupe, M. D. (2015). Humidity trends imply increased sensitivity to clouds in a warming Arctic. *Nature Communications*, *6*(1), 1–8. https://doi.org/10.1038/ncomms10117

Crane, R., & Hewitson, B. (2003). Clustering and upscaling of station precipitation records to regional patterns using self-organizing maps (SOMs). *Climate Research*, *25*(2), 95–107. https://doi.org/10.3354/cr025095

Enderlin, E. M., Howat, I. M., Jeong, S., Noh, M. J., Van Angelen, J. H., & Van Den Broeke, M. R. (2014). An improved mass budget for the Greenland ice sheet. *Geophysical Research Letters*, *41*, 866–872. https://doi.org/10.1002/2013GL059010

Fettweis, X., Franco, B., Tedesco, M., Van Angelen, J. H., Lenaerts, J. T., Van Den Broeke, M. R., & Gall´ee, H. (2013). Estimating the Greenland ice sheet surface mass balance contribution to future sea level rise using the regional atmospheric climate model MAR. *The Cryosphere*, *7*(2), 469–489. https://doi.org/10.5194/tc-7-469-2013

Franco, B., Fettweis, X., & Erpicum, M. (2013). Future projections of the Greenland ice sheet energy balance driving the surface melt. *The Cryosphere*, *7*(1), 1–18. https://doi.org/10.5194/tc-7-1-2013

Gallagher, M., Shupe, M. D., & Miller, N. B. (2018). Impact of atmospheric circulation on temperature, clouds, and radiation at Summit Station, Greenland with self-organizing maps. *Journal of Climate*, *31*, 8895–8915. https://doi.org/10.1175/JCLI-D-17-0893.1

Guzman, R., Chepfer, H., Noel, V., de Gu´elis, T. V., Kay, J. E., Raberanto, P., et al. (2017). Direct atmosphere opacity observations from CALIPSO provide new constraints on cloud-radiation interactions. *Journal of Geophysical Research: Atmospheres*, *122*, 1066–1085. https://doi.org/10.1002/2016JD025946

Hofer, S., Tedstone, A. J., Fettweis, X., & Bamber, J. L. (2017). Decreasing cloud cover drives the recent mass loss on the Greenland ice sheet. *Science Advances*, *3*(6), e1700584. https://doi.org/10.1126/sciadv.1700584

Kalnay, E., Kanamitsu, M., Kistler, R., Collins, W., Deaven, D., Gandin, L., et al. (1996). The NCEP/NCAR 40-year reanalysis project. *Bulletin of the American Meteorological Society*, *77*(3), 437–471. https://doi.org/10.1175/1520-0477(1996)077(0437:TNYRP)2.0.CO;2

Kay, J. E., & L'Ecuyer, T. (2013). Observational constraints on Arctic Ocean clouds and radiative fluxes during the early 21st century. *Journal of Geophysical Research: Atmospheres*, *118*, 7219–7236. https://doi.org/10.1002/jgrd.50489

Kay, J. E., L'Ecuyer, T., Chepfer, H., Loeb, N., Morrison, A., & Cesana, G. (2016). Recent advances in Arctic cloud and climate research. *Current Climate Change Reports*, *2*(4), 159–169. https://doi.org/10.1007/s40641-016-0051-9

Kohonen, T. (2013). Essentials of the self-organizing map. *Neural Networks*, *37*, 52–65. https://doi.org/10.1016/j.neunet.2012.09.018

Lacour, A., Chepfer, H., Miller, N. B., Shupe, M. D., Noel, V., Fettweis, X., et al. (2018). How well are clouds simulated over Greenland in climate models? Consequences for the surface cloud radiative effect over the ice sheet. *Journal of Climate*, *31*(22), 9293–9312. https://doi.org/10.1175/JCLI-D-18-0023.1

Lenaerts, J. T., Van Tricht, K., Lhermitte, S., & L'Ecuyer, T. S. (2017). Polar clouds and radiation in satellite observations, reanalyses, and climate models. *Geophysical Research Letters*, *44*, 3355–3364. https://doi.org/10.1002/2016GL072242

Mattingly, K. S., Mote, T. L., & Fettweis, X. (2018). Atmospheric river impacts on Greenland ice sheet surface mass balance. *Journal of Geophysical Research: Atmospheres*, *123*, 8538–8560. https://doi.org/10.1029/2018JD028714

Miller, N. B., Shupe, M. D., Cox, C. J., Noone, D., Persson, P. O. G., & Steffen, K. (2017). Surface energy budget responses to radiative forcing at Summit, Greenland. *The Cryosphere*, *11*(1), 497–516. https://doi.org/10.5194/tc-11-497-2017

Mioduszewski, J. R., Rennermalm, A. K., Hammann, A., Tedesco, M., Noble, E. U., Stroeve, J. C., & Mote, T. L. (2016). Atmospheric drivers of Greenland surface melt revealed by self-organizing maps. *Journal of Geophysical Research: Atmospheres*, *121*, 5095–5114. https://doi.org/10.1002/2015JD024550

Morrison, A. L., Kay, J. E., Chepfer, H., Guzman, R., & Yettella, V. (2018). Isolating the liquid cloud response to recent Arctic sea ice variability using spaceborne lidar observations. *Journal of Geophysical Research: Atmospheres*, *123*, 473–490. https://doi.org/10.1002/2017JD027248

Neff, W., Compo, G. P., Martin Ralph, F., & Shupe, M. D. (2014). Continental heat anomalies and the extreme melting of the Greenland ice surface in 2012 and 1889. *Journal of Geophysical Research: Atmospheres*, *119*, 6520–6536. https://doi.org/10.1002/2014JD021470

Nghiem, S. V., Hall, D. K., Mote, T. L., Tedesco, M., Albert, M. R., Keegan, K., et al. (2012). The extreme melt across the Greenland ice sheet in 2012. *Geophysical Research Letters*, *39*, L20502. https://doi.org/10.1029/2012GL053611

Oltmanns, M., Straneo, F., & Tedesco, M. (2019). Increased Greenland melt triggered by large-scale, year-round cyclonic moisture intrusions. *The Cryosphere*, *13*(3), 815–825. https://doi.org/10.5194/tc-13-815-2019

Pedregosa, F., Varoquaux, G., Gramfort, A., Michel, V., Thirion, B., Grisel, O., et al. (2011). Scikit-learn: Machine learning in Python. *Journal of Machine Learning Research*, *12*, 2825–2830.

Riihelä, A., King, M. D., & Anttila, K. (2019). The surface albedo of the Greenland ice sheet between 1982 and 2015 from the Clara-A2 dataset and its relationship to the ice sheet's surface mass balance. *The Cryosphere*, *13*(10), 2597–2614. https://doi.org/10.5194/tc-13-2597-2019

Schuenemann, K. C., & Cassano, J. J. (2009). Changes in synoptic weather patterns and Greenland precipitation in the 20th and 21st centuries: 1. Evaluation of late 20th century simulations from IPCC models. *Journal of Geophysical Research*, *114*, D20113. https://doi.org/10.1029/2009JD011705

Sedlar, J., Tjernström, M., Mauritsen, T., Shupe, M. D., Brooks, I. M., Persson, P. O. G., et al. (2011). A transitioning Arctic surface energy budget: The impacts of solar zenith angle, surface albedo and cloud radiative forcing. *Climate Dynamics*, *37*(7-8), 1643–1660. https://doi.org/10.1007/s00382-010-0937-5

Serreze, M. C., & Barry, R. G. (2011). Processes and impacts of Arctic amplification: A research synthesis. *Global and Planetary Change*, *77*(1-2), 85–96. https://doi.org/10.1016/j.gloplacha.2011.03.004

Shepherd, A., Ivins, E. R., A, G., Barletta, V. R., Bentley, M. J., Bettadpur, S., et al. (2012). A reconciled estimate of ice-sheet mass balance. *Science (80)*, *338*(6111), 1183–1189. https://doi.org/10.1126/science.1228102

Sheridan, S. C., & Lee, C. C. (2011). The self-organizing map in synoptic climatological research. *Progress in Physical Geography*, *35*(1), 109–119. https://doi.org/10.1177/0309133310397582

Shupe, M. D., & Intrieri, J. M. (2004). Cloud radiative forcing of the Arctic surface: The influence of cloud properties, surface albedo, and solar zenith angle. *Journal of Climate*, *17*(3), 616–628. https://doi.org/10.1175/1520-0442(2004)017(0616:CRFOTA)2.0.CO;2

Shupe, M. D., Turner, D. D., Zwink, A., Thieman, M. M., Mlawer, E. J., & Shippert, T. (2015). Deriving arctic cloud microphysics at Barrow, Alaska: Algorithms, results, and radiative closure. *Journal of Applied Meteorology and Climatology*, *54*(7), 1675–1689. https://doi.org/10.1175/JAMC-D-15-0054.1

Solomon, A., Shupe, M. D., & Miller, N. B. (2017). Cloud-atmospheric boundary layer-surface interactions on the Greenland ice sheet during the July 2012 extreme melt event. *Journal of Climate*, *30*(9), 3237–3252. https://doi.org/10.1175/JCLI-D-16-0071.1

Steffen, K., Box, J., & Abdalati, W. (1996). Greenland climate network: GC-Net. US Army Cold Regions Reattach and Engineering (CRREL), CRREL Special Report, 98–103.

Stone, R. S. (1997). Variations in western Arctic temperatures in response to cloud radiative and synoptic-scale influences. *Journal of Geophysical Research*, *102*(D18), 21,769. https://doi.org/10.1029/97JD01840

Vaillant de Gúelis, T., Chepfer, H., Noel, V., Guzman, R., Winker, D. M., & Plougonven, R. (2017). Using space lidar observations to decompose longwave cloud radiative effect variations over the last decade. *Geophysical Research Letters*, *44*, 11,994–12,003. https://doi.org/10.1002/2017GL074628

Van As, D. (2011). Warming, glacier melt and surface energy budget from weather station in the Melville Bay Greenland. *Journal of Glaciology*, *57*(202), 1–13. https://doi.org/10.3189/002214311796405898

van den Broeke, M., Bamber, J., Ettema, J., Rignot, E., Schrama, E., van de Berg, W. J., et al. (2009). Partitioning recent Greenland mass loss. *Science*, *326*(5955), 984–986. https://doi.org/10.1126/science.1178176

Van Tricht, K., Lhermitte, S., Lenaerts, J. T., Gorodetskaya, I. V., L'Ecuyer, T. S., Noël, B., et al. (2016). Clouds enhance Greenland ice sheet meltwater runoff. *Nature Communications*, *7*(1), 10266. https://doi.org/10.1038/ncomms10266

Young, G. H., McCarroll, D., Loader, N. J., Gagen, M. H., Kirchhefer, A. J., & Demmler, J. C. (2012). Changes in atmospheric circulation and the Arctic Oscillation preserved within a millennial length reconstruction of summer cloud cover from northern Fennoscandia. *Climate Dynamics*, *39*(1-2), 495–507. https://doi.org/10.1007/s00382-011-1246-3